

Article

Surface Enhancement of Titanium-Based Coatings on Commercial Hard Steel Cutting Tools

Minh Nhat Dang ^{1,2,*} , Surinder Singh ¹ , Hannah J. King ¹ , John H. Navarro-Devia ³ , Hoang Le ⁴, Thomas G. Pattison ¹, Rosalie K. Hocking ¹, Scott A. Wade ¹ , Guy Stephens ³, Angelo Papageorgiou ³, Armando Manzano ² and James Wang ^{1,*}

¹ The Australian Research Council (ARC) Training Centre in Surface Engineering for Advanced Materials (SEAM), School of Engineering, Swinburne University of Technology, P.O. Box 218, Hawthorn, VIC 3122, Australia; surindersingh@swin.edu.au (S.S.); hjking@swin.edu.au (H.J.K.); tpattison@swin.edu.au (T.G.P.); rhocking@swin.edu.au (R.K.H.); swade@swin.edu.au (S.A.W.)

² ANCA Pty Ltd., 25 Gatwick Rd, Bayswater North, VIC 3153, Australia

³ Sutton Tools, 378 Settlement Rd, Thomastown, VIC 3074, Australia; jnavarro@sutton.com.au (J.H.N.-D.); apapageorgiou@sutton.com.au (A.P.)

⁴ The Electron Microscopy and Materials Analysis Research Group, School of Computing and Engineering, University of Huddersfield, Queensgate, Huddersfield HD1 3DH, UK; hoang.le@hud.ac.uk

* Correspondence: nhatminh@swin.edu.au (M.N.D.); jawang@swin.edu.au (J.W.)

Abstract: This study investigates the mechanical properties, surface integrity, and chemical configuration of PVD-coated high-speed steel (HSS) cutting tools, with a particular focus on titanium nitride (TiN) and titanium aluminium nitride (TiAlN) coatings. A range of characterisation methodologies were employed to examine the impact of pre-coating surface conditions on the resulting coatings. This impact includes the effects of gas bubble production and unequal distribution of elements, which are two unwanted occurrences. Notwithstanding these difficulties, coatings applied on surfaces that were highly polished exhibited more consistency in their mechanical and elemental characteristics, with a thickness ranging from 2 to 4 µm. The study of mechanical characteristics confirms a significant increase in hardness, from an initial value of roughly 1000 HV0.5 for untreated tools to 1300 HV0.5 for tools with physical vapour deposition (PVD) coatings. Although PVD coatings produced on an industrial scale might not exceed the quality of coatings manufactured in a laboratory, they do offer substantial enhancements in terms of hardness. This study highlights the significant importance of thorough surface preparation in achieving enhanced coating performance, hence contributing to the efforts to prolong the lifespan of tools and enhance their performance even under demanding operational circumstances.

Keywords: thin film coating; cutting tools; titanium nitride; aluminium nitride; surface finish; high speed steel; PVD



Citation: Dang, M.N.; Singh, S.; King, H.J.; Navarro-Devia, J.H.; Le, H.; Pattison, T.G.; Hocking, R.K.; Wade, S.A.; Stephens, G.; Papageorgiou, A.; et al. Surface Enhancement of Titanium-Based Coatings on Commercial Hard Steel Cutting Tools. *Crystals* **2024**, *14*, 470. <https://doi.org/10.3390/cryst14050470>

Academic Editor: George D. Verros

Received: 9 March 2024

Revised: 11 May 2024

Accepted: 14 May 2024

Published: 17 May 2024



Copyright: © 2024 by the authors. Licensee MDPI, Basel, Switzerland. This article is an open access article distributed under the terms and conditions of the Creative Commons Attribution (CC BY) license (<https://creativecommons.org/licenses/by/4.0/>).

1. Introduction

Research into high-performance materials and surface engineering techniques has intensified due to the constant demand for advances in productivity and durability. This demand is exemplified in cutting tool research. Due to their beneficial mechanical properties, such as high working hardness with excellent toughness, high-speed steel (HSS) cutting tools have remained an everyday commodity in manufacturing applications [1,2]. The adoption of elegant surface treatments, such as thin-film coatings, particularly nitride-based coatings, can further improve their performance [3–7].

TiN, TiCN, and TiAlN are common hard coatings used to extend the operational life of HSS tools. Composed of nitrogen, titanium, and other additive elements such as carbon, aluminium, silicon, and chromium, these coatings offer a variety of advantages [8]. In general, the deposition procedure involves chemical vapour deposition (CVD), physical

vapour deposition (PVD), or a hybrid technique [9]. While CVD methods can accomplish coating thicknesses greater than 20 μm , PVD typically produces coatings with a thickness of just a few microns [7,10,11].

For over six decades, titanium nitride (TiN) has been extensively used in coating tools, particularly HSS tools, to increase the production rate, product quality, and tool life. TiN is a golden yellow ceramic with low density (5.22 g/cm³), high melting point (>2900 °C), high hardness (20–50 GPa), superconductivity ($\sim 15 \mu\Omega\cdot\text{cm}$), and chemical resistivity at ambient conditions (>400 °C to become oxidised) [12–16]. With the TiN coating, the life of tool steel could be increased from two- to over ten-fold in some cases [17]. However, the presence of titanium residue potentially decreases the wear resistance of the coating layer. For a continuous cutting motion, a thicker TiN coating is favourable for a longer tool life. But for a discontinuous cutting motion (e.g., planning or turning), TiN film has a corresponding optimal thickness [18].

A range of elements in the carbon family, i.e., group 14 in the periodic table, are doped into the TiN matrix to form intermetallics, which have superior properties compared to bare TiN for specific purposes [19–21]. Examples include Ti-B-N, Ti-C-N, Ti-Si-N, Ti-Al-N to Ti-Si-B-N, Ti-Al-C-N, and Ti-Al-Cr-N. When the ratio and chemical composition are changed, the resulting coatings inherit different structural, mechanical, and tribological characteristics [22,23]. For example, Ti-Al-N exhibits considerably higher oxidative resistance than TiN coatings [24]. As the oxygen ions in the air can easily penetrate the TiO₂ layer, if enough Al content is added, the oxide layer on top of the tool surface can be self-healed when the surrounding temperature is high, especially when the tool works in a high-speed condition. This in turn eliminates any negative effect on the overall hardness of the tool [3]. Coated tools are especially beneficial for mitigating the mechanical and thermal stresses caused by high-speed machining processes [8,25]. They reduce tool-chip friction and interactions, thereby increasing cost-effectiveness and machining output. A study by Vannan et al. further supports these claims, demonstrating that tools coated with an AlCrN and TiAlN bilayer obtained a 50% reduction in machining duration, 580% longer life, a 130% harder surface, and 36% finer surface roughness when compared to an uncoated tool [26].

Despite the considerable body of research and apparent comprehension of the characteristics of TiN and other nitride coatings in laboratory settings, a significant disparity persists in their practical use within industrial contexts. The features of lab-synthesised coatings are generally characterised by their idealised nature, which can be attributed to the controlled environment provided by the deposition techniques commonly employed in research conditions. However, the practical effectiveness of coatings produced using industrial-scale PVD systems may not always align with the ideal outcomes, hence raising concerns about their overall performance. The aforementioned discrepancy highlights the necessity for a thorough assessment of commercially accessible high-speed steel cutting tools that undergo coating through industrial PVD systems. Hence, conducting a broad analysis of commercially coated HSS tools is both opportune and important in order to effectively translate academic progress into tangible industrial advantages. By addressing this research gap, it is possible to develop a more accurate comprehension of coating integrity that will lead to enhanced tool performance and manufacturing productivity optimisation. Herein, the purpose of our study is to contribute to the current reservoir of knowledge by providing an in-depth examination of the nature of titanium-nitride-based coatings on the surface integrity of industrial cutting tools.

2. Materials and Methods

The M2 HSS cutting tools and steel flat substrates used in this investigation were supplied by Sutton Tools (Thomastown, Australia). Several external industry partners offered TiN and TiAlN thin-film coatings for the tool steel. The parameters of the coating deposition process are kept confidential to prevent any potential copyright infringement. Before additional microstructural analysis was conducted, the tool samples were cut into

cross-sections using a Struer's B0D20 diamond-embedded cutting disc with a Setocom-50 cutter machine. The cutting was performed at the default direct-cut speed of 2200 rpm and a cutting speed of 0.060 mm/s. The cut samples were subsequently mounted with an epoxy resin mixture at low temperatures for a duration of 48 h. The samples that were attached to a mount were subsequently polished using SiC #220 to #1200 grinding papers and DiaPro 9 μm and 6 μm diamond suspensions from Struers (Queensland, Australia), depending on the specific analysis technique being employed.

BX61 digital microscopes equipped with a $50\times$ Olympus lens and automatic exposure were used to capture optical microscope images. A Zeiss Supra 40 VP FE-SEM was used to perform scanning electron microscopy (SEM) analysis at 5 kV. Its purpose in this study was to characterise cross-sectioned samples. The specimens were divided into longitudinal and transverse sections, which were then cleaned with distilled water and acetone. The sections were then affixed to a copper substrate using carbon adhesive. Using the energy-dispersive X-ray spectroscopy (EDX) technique, an Oxford Instruments INCAxcat detector was employed to analyse both sample materials. The analysis was conducted using a voltage of 20 kV for secondary electron and back-scattering electron (BSE) detectors. Each scan took approximately 3 min, and there were 5 relocating scans per spot.

The lamellae from the three ODS-FeCrAl alloys were extracted using a focused ion beam (FIB) technique prior to transmission electron microscopy (TEM). The extraction process was performed using an FEI Quanta 200 3D FIB system, which operated at 30 kV and utilised Ga^+ ions. Subsequently, the extracted lamellae were positioned onto Mo support grids in preparation for high-temperature in situ ion irradiations. The samples underwent verification using energy-filtered transmission electron microscopy (EFTEM) to confirm that they had been further reduced to a final thickness of approximately 100 nm. A final focused ion beam (FIB) step was performed using 5 kV gallium ions (Ga^+) to ensure a pristine surface suitable for high-resolution transmission electron microscopy (TEM) investigations. The TEM experiments were conducted using a Hitachi H-9500 system operating at 300 kV. The samples underwent a pre-cleaning process in which they were washed with ethanol to eliminate any impurities on the surface.

The Raman spectroscopy analysis was conducted using a Renishaw[®] confocal InVia Raman Microscope system located in Gloucestershire, UK. WIRE[™] software v4.4.1 was utilised in the system to perform both the acquisition of spectra and the subtraction of baselines. The user combined a 50 L Olympus lens with a laser emitting light at a wavelength of 633 nm. Each Raman scan was conducted with a 20 s exposure time, utilising the full 150 W laser power and 20 accumulations.

X-ray diffraction (XRD) measurements were conducted using a Bruker D8 Advanced Eco diffractometer, equipped with a 1 kW copper (Cu) X-ray source operating at 40 kV and 25 mA. To maintain a consistent sample irradiation area of 10 mm², a variable aperture was employed, along with a 2.5° Soller module and a stationary 2 mm air screen. The LYNXEYE XY T detector was utilised in one-dimensional mode. The scan parameters ranged from 5° to 100°, with an increment of 0.02°, a duration of 0.5 s per increment, and no sample rotation. The data were collected using the Bragg–Brentano geometry in a continuous mod, and subsequently analysed using the DIFFRAC.EVA software v2 to assess the crystalline structures and phase compositions.

A 3D optical profilometer was used to scan the surface topography of the samples in three dimensions. In order to remove any impurities, the surface of all samples underwent an initial cleaning process in an ultrasonication bath, utilising a mixture of deionised (DI) water and acetone. The surface of the sample was later examined using a Bruker ContourGT-X 3D Optical Profiler in VSI mode, with a $50\times$ magnification. The roughness data were subsequently analysed using Vision84 software v5.6, which conforms to the ISO 4288 standard [27]. Ten random measurements were conducted for each sample to ensure statistically significant results, followed by the calculation of roughness and standard deviation. The average roughness of specific samples was determined by conducting a scan over a 0.5×0.5 mm area using stitching mode.

A Duramin-40 Vickers Hardness Tester was utilised to conduct microhardness testing. The instrument is furnished with a diamond indenter capable of applying precise loads of 300 gf for flat samples and 500 gf for complex tool samples. It also has a dwell time of 10 s and a high-resolution camera for capturing images of the indents, which can be analysed later. The machine is equipped with Duramin software, which automatically calculates hardness values based on the size of the indentations.

3. Results and Discussion

The preliminary examination of the TiN coated on a HSS tool using electron microscopy indicated the presence of a significant number of surface imperfections in different areas of the tool, particularly well-known micro-chipping at the cutting edge (Figure 1). These defects seem to result from the inherent imperfections in the grinding textures, which remain visible even after the coating process. Additionally, the occurrence of gas bubble formation, a widely recognised problem in TiN coatings resulting from PVD processes, was noticed. There could be many possible reasons for this bubble formation, such as surface contamination, overgrowth, moisture accumulation, or disrupted thermal gradients across the coated surface [28]. During the process of deposition, any surplus nitrogen can either occupy unoccupied lattice sites within the material or form precipitates at the boundaries between grains, as well as manifesting as gas bubbles. The presence of polyhedral nitrogen bubbles supports the conclusions drawn from previous studies on single-crystal TiN films that were produced through bias sputtering under a pure N₂ atmosphere [29]. The surface quality displayed a regional variation, with the outer regions (such as the cutting edge and shank areas) exhibiting relatively higher smoothness, while the flute valleys demonstrated rougher characteristics. The observed difference can be ascribed to the naturally occurring limitations of mechanical polishing methods, which exhibit reduced efficacy in reaching recessed geometries, resulting in non-uniform pre-coating surfaces. As a result, although the deposition parameters were carefully controlled to achieve a uniform thickness, the resulting TiN coating exhibited a similar level of high roughness. The utilisation of EDX enabled the observation of a non-homogeneous dispersion of titanium, with a notable reduction in the valley regions. This phenomenon can be attributed to the limited accessibility of sputtered atoms to these specific areas. Moreover, the existence of oxygen remnants in the valley regions can be attributed to the inadequate pairing of titanium with nitrogen during the sputtering procedure, subsequently causing the creation of titanium oxides upon contact with atmospheric oxygen. The utilisation of digital microscopy in a cross-sectional analysis provided confirmation that the TiN coating, with an average thickness of 2–3 µm, accurately replicated the underlying surface topography while maintaining a uniform layer thickness. A post-deposition inspection of the TiAlN-coated tool sample reveals a similar heterogeneous surface topology, with the highest surface quality present in the shank and the worst in the valleys (Figure 2). The elements that make up the coating are unevenly distributed, as shown by elemental mapping; the titanium concentration is especially low in valley regions. The results for the TiN-coated sample are supported by these observations of non-uniformity, which highlight the shortcomings of current mechanical polishing methods in preparing complex geometries for coating processes. Evidently, the coating that is applied on top depends on the quality of the surface beneath it. Figure 3, which displays TiAlN-coated samples with both flat and complicated geometries, shows that a finer post-coating texture results from a smoother pre-coating surface. The coating thickness is uniform across both sample types, averaging around 2 µm. Additionally, this discovery highlights the capability of the deposition approach to maintain a uniform thickness, even across complicated topographies, confirming the significance of surface preparation prior to the coating process.

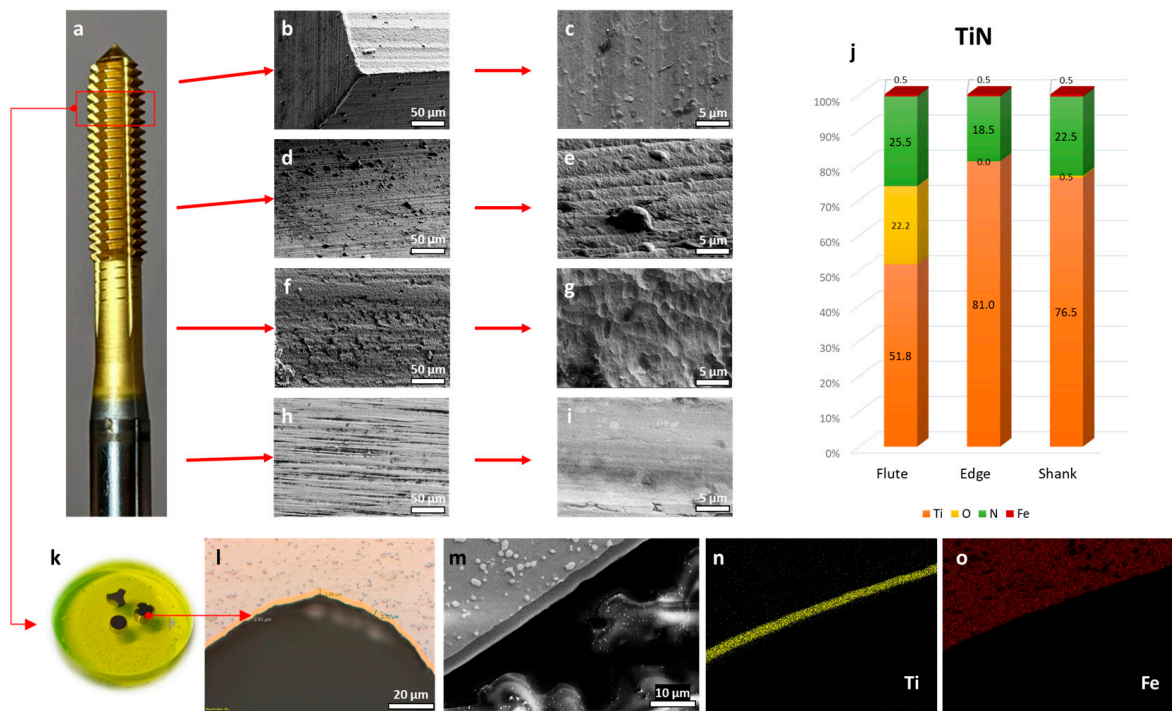


Figure 1. (a) Photograph of TiN coated on HSS tool. Four regions of the tool were examined: the cutting edge, the flute valley, the shank, and an uncoated area. Data from these four regions are presented as (b–i) SEM images from (b,c) the cutting edge, (d,e) the flute valley, (f,g) the shank, and (h,i) the uncoated area and (j) the elemental distribution (wt%) from EDX data. (k) Photograph of the cross-sectional cuts of the TiN tool mounted in epoxy, with data from the coated region presented as (l) an optical microscope image, (m) an SEM image, and (n,o) elemental maps of Ti and Fe from EDX.

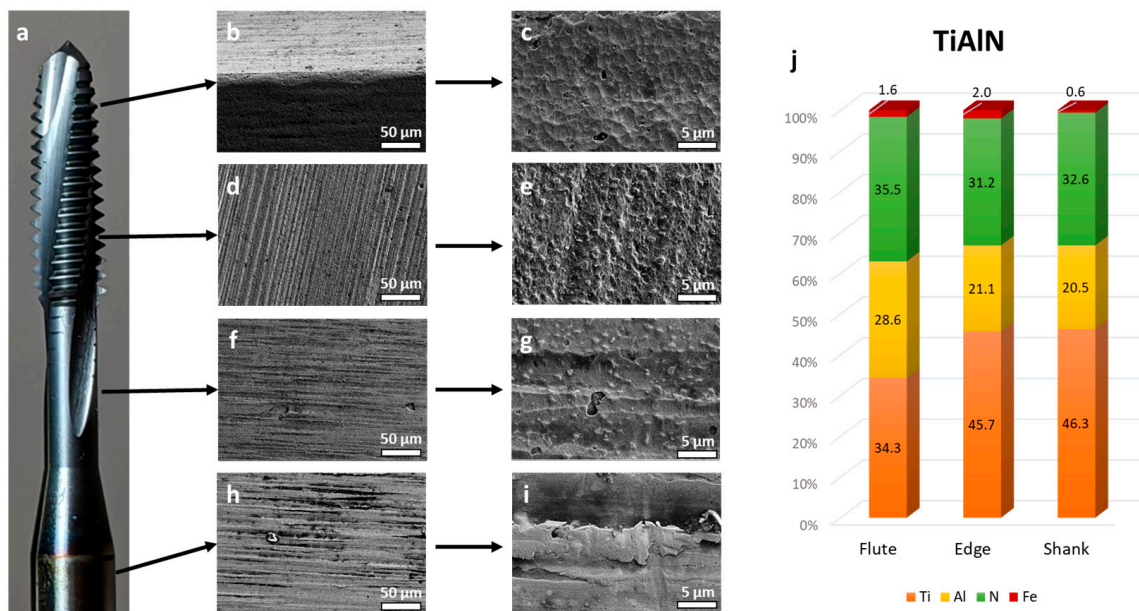


Figure 2. (a) Photograph of TiAlN-coated tool sample. Four regions of the tool were examined: the cutting edge, the flute valley, the shank, and an uncoated area. Data from these four regions are presented as (b–i) SEM images from (b,c) the cutting edge, (d,e) the flute valley, (f,g) the shank, and (h,i) an uncoated area and (j) elemental distribution (wt%) from EDX data.

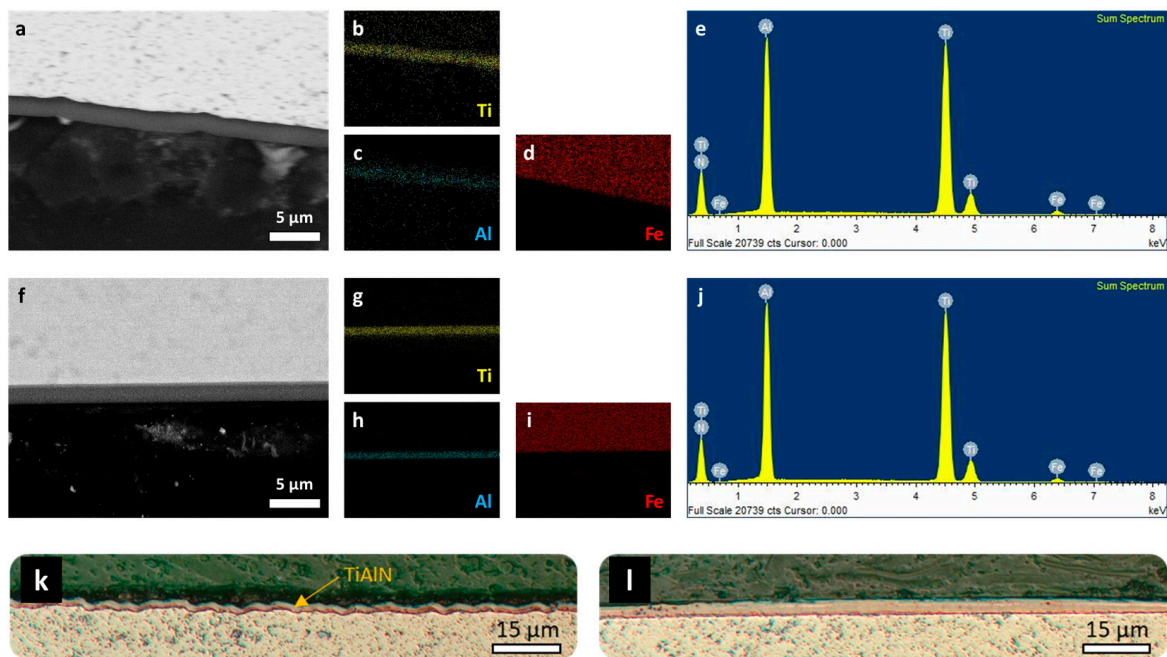


Figure 3. SEM, BSE EDX, and optical microscopy data of cross-sectional (a–e,k) complex tool and (f–j,l) flat substrate samples coated with TiAlN thin film.

Despite the enhanced surface quality achieved through improved polishing techniques, the process of coating deposition inherently leads to an increase in surface roughness. This is evidenced by the findings of 3D profilometry scans performed on flat steel samples (Figure 4). The original arithmetic mean roughness (R_a) of the raw surface was determined to be 20.9 ± 8.0 nm. Following the application of a TiN coating, the roughness increased to 39.3 ± 5.0 nm. Subsequently, after the deposition of a TiAlN coating, the roughness was measured at 32.5 ± 7.2 nm. The root mean square roughness (R_q) demonstrated a comparable pattern, with a rise from an initial measurement of 28.0 ± 7.4 nm to 60.0 ± 7.2 nm for surfaces coated with TiN and 72.2 ± 26.1 nm for surfaces coated with TiAlN. Significantly, there was a meaningful increase in R_z measurement data. Specifically, the raw surface exhibited a value of 3.8 ± 1.2 μm , while the TiN coating showed an elevation of 6.3 ± 1.3 μm , and the TiAlN coating showed the highest elevation of 7.6 ± 1.5 μm . While the thicknesses of both coatings are alike, TiAlN encounters a lower average roughness but displays a greater number of peaks and valleys in its surface texture compared to TiN.

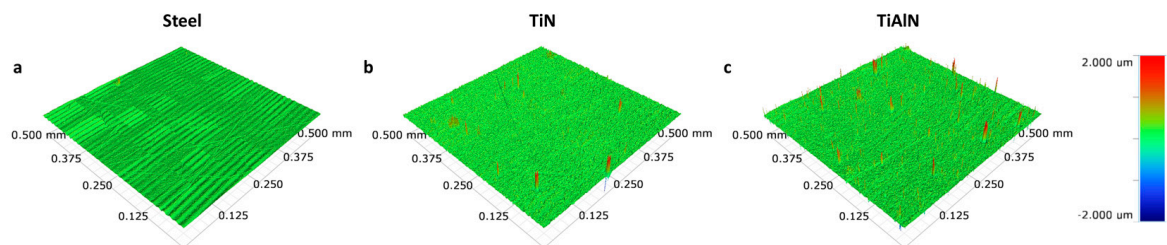


Figure 4. Three-dimensional profilometer scans of flat (a) raw steel substrate, (b) TiN-coated substrate, and (c) TiAlN-coated substrate.

Furthermore, an assessment of the mechanical properties of these coatings was conducted by employing the Vickers microhardness test on flat coated samples. A significant increase in hardness was observed in the investigation. Particularly, the hardness of the flat steel substrate jumped from an initial value of 444.9 ± 14.3 HV0.3 to 601.9 ± 12.6 HV0.3 with the application of a TiN coating. Furthermore, the hardness further increased to

738.0 ± 30.7 HV0.3 with TiAlN coating. The addition of aluminium to the titanium nitride lattice greatly enhances the mechanical strength of the coating, as demonstrated by the notable rise in hardness. The appearance of differences in hardness distribution for each sample is depicted in Figure 5, using gradient colours that are aligned with the corresponding scale bar. Both TiN and TiAlN coatings offer a more consistently homogeneous harder surface in comparison with the raw steel substrate.

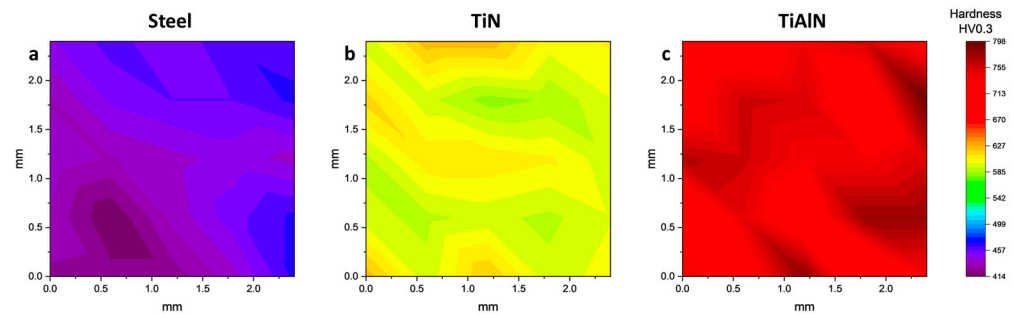


Figure 5. Hardness distribution of flat (a) steel substrate, (b) TiN-coated sample, and (c) TiAlN-coated sample.

The chemical configuration of thin-film TiN and TiAlN coatings is revealed through the application of Raman spectroscopic analysis, as seen in Figure 6. The presence of peaks at 667 and 800 cm^{-1} in the substrate's spectrum indicates the corrosion of iron and the main additive element, molybdenum, which can be attributed to prolonged exposure to ambient oxygen [30–32]. The TiN and TiAlN films exhibit five wide spectral bands ranging from 100 to 1000 cm^{-1} . The initial two phonon bands of the acoustic area, which are associated with longitudinal acoustic (LA) and transverse acoustic (TA) vibrations, exhibit frequencies of 215 and 324 cm^{-1} for TiN and 246 and 345 cm^{-1} for TiAlN. The longitudinal optic (LO) and transverse optic (TO) bands, which are located in the optic region, have corresponding central frequencies of 562 and 646 cm^{-1} , which are assigned for TiN and TiAlN, respectively. The spectral characteristics, observed within the reported range according to previous TiN studies, can often be ascribed to the vibrational modes of titanium and nitrogen ions in the acoustic and optic domains, respectively [33–35]. The detected deviations in the peak positions of TiN and TiAlN suggest the presence of slight alterations in the levels of vacancies [36]. This is further supported by a semi-quantitative analysis of the intensity ratio between titanium and nitrogen peaks, which is found to be greater in TiN. These vacancies likely originate from slight oxidation events of titanium, facilitated by possible residual oxygen in the industrial deposition chamber, and are partly compensated by the presence of alumina, or even aluminium nitrides [37–39]. Although TiN has a well-ordered FCC structure, which theoretically limits first-order Raman scattering, the presence of defects from the industrial coating process disrupts this symmetry. TiAlN coatings exhibit a pronounced increase in the intensity of phonon bands compared to their binary TiN counterparts. This heightened intensity, which was already four-fold reduced to be included in this graph, can be attributed to the presence of a secondary heavier ion—aluminium [40]. In addition to the aforementioned spectral characteristics, the presence of second-order acoustic bands at 434 and 479 cm^{-1} was observed for TiN and TiAlN, respectively. Furthermore, higher frequency peaks at 787 and 779 cm^{-1} can be attributed to second-order transitions [41]. The presented results illustrate the inherent intricacy and regular imperfections observed in PVD coatings produced on an industrial scale, in contrast to the more controlled synthesis methods employed in laboratory settings.

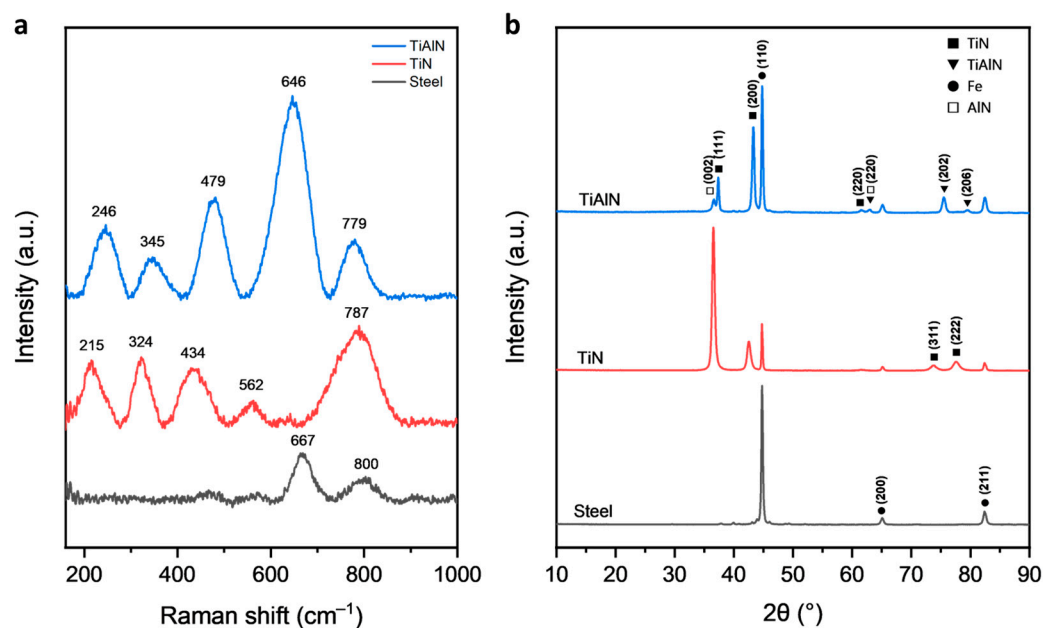


Figure 6. (a) Raman and (b) XRD spectra of raw steel substrate and TiN- and TiAlN-coated samples.

X-ray diffraction spectroscopy was employed to extensively investigate the crystalline phases of the coated samples. The raw steel substrate exhibited three distinct iron phases on the (110), (200), and (211) reflection planes, which also appear in the nitride coatings due to the X-ray penetration depth exceeding the coating thickness [42–44]. In accordance with its FCC phase, the TiN coating primarily exhibited strong diffraction peaks at 36.6 and 42.6°, corresponding to the (111) and (200) planes [45,46]. Weak peaks at 73.8 and 77.6° can be attributed to the (311) and (222) planes, respectively, as confirmed in previous studies [47–49]. Both TiAlN and TiN coatings exhibit (111) orientation, in which surfaces terminated by nitrogen (N) atoms displayed a more pronounced inward relaxation compared to those terminated by titanium (Ti) atoms, but TiAlN exhibited a broader and less intense diffraction pattern for the (111) and (200) planes, which are TiN’s preferred orientations [50,51]. This could be caused by internal lattice strain or defect-induced broadening. When compared to TiN, the TiAlN (111) peak exhibited a slight shift towards higher angles, possibly due to the incorporation of aluminium-based lattice modes [52]. Furthermore, the intensity of the (200) peak in TiAlN is higher than the (111) peak of the same sample but lower than that of TiN. In the TiAlN sample, minor peaks corresponding to TiN’s (220) plane are close to the AlN cubic (220) plane, while the h-AlN (002) plane peaks at 36.6° [51,53,54]. Furthermore, hexagonal TiAlN phases were discovered on the (202) and (206) planes, the latter of which could be related to the alumina phase on the (220) plane at 79.5° [51,55]. As a result, the industrial TiAlN coating appears to consist of four distinct structures: cubic TiN, hexagonal TiAlN, AlN, and perhaps Al₂O₃, which is supported by their respective Raman spectral modes. The complex multiphase and poly-crystalline structure of the TiAlN-coated tool sample is further elucidated through TEM (Figure 7). The detected lattice size of 0.21 nm was identified as corresponding to the (200) crystal plane of TiN [56]. The presence of discrete clusters of cubic TiN within the TiAlN matrix suggests an inconsistent arrangement of phases. The recurring dark and bright layers observed in the TEM micrographs correspond to the TiN and TiAlN layers, respectively. The TiAlN and AlN layers exhibit slightly brighter regions in comparison to the TiN layers due to the lower scattering factor attributed to aluminium ions [57].

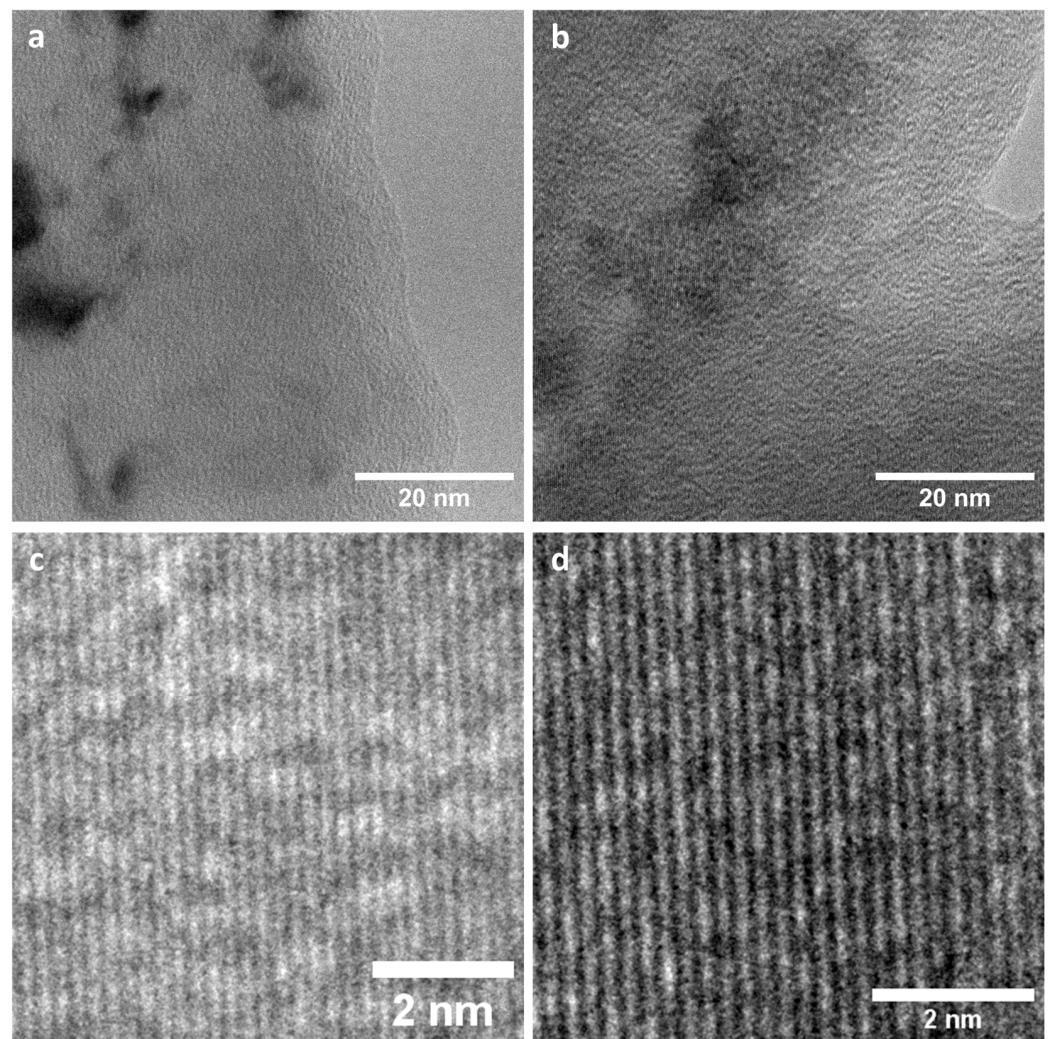


Figure 7. TEM images of (a,c) TiN and (b,d) TiAlN tool samples.

As part of a further inquiry, we conducted an investigation of alternative coatings, specifically those based on nitrides and diamond-like carbon, applied to identical tool substrates in order to ascertain their respective surface qualities. While the examination conducted for these extra coatings was only preliminary, it offers valuable insights that support our conclusions. Figures 8 and 9 provide a quick overview of elemental, mechanical, and crystallographic characteristics, as well as morphological aspects. Significantly, the application of these coatings resulted in substantial enhancements in hardness, raising the Vickers hardness value from an initial measurement of roughly 1000 HV0.5 for uncoated HSS to over 1300 HV0.5. The sample coated with TiAlSiN had the most significant increase in hardness, as well as the highest surface roughness, resulting in an almost two-fold increase in the Ra value compared to the uncoated substrate. The aforementioned observations are consistent with the findings reported in previous scholarly works, providing more evidence for the occurrence of TiN and AlN layers inside the majority of TiAlN-based coatings [11,27,51,58–61]. In addition, the inclusion of SEM images and 3D profilometer scans confirmed that the coatings accurately replicated the roughness of the surface to which they were deposited. This allowed for the identification of various imperfections such as microchipping and residual grinding textures that may have resulted from previous polishing and machining processes. Also, the formation of bubbles and holes is observable on these coating surfaces. Therefore, although these coatings had improved mechanical durability, they also amplified surface imperfections, a phenomenon that warrants further investigation.

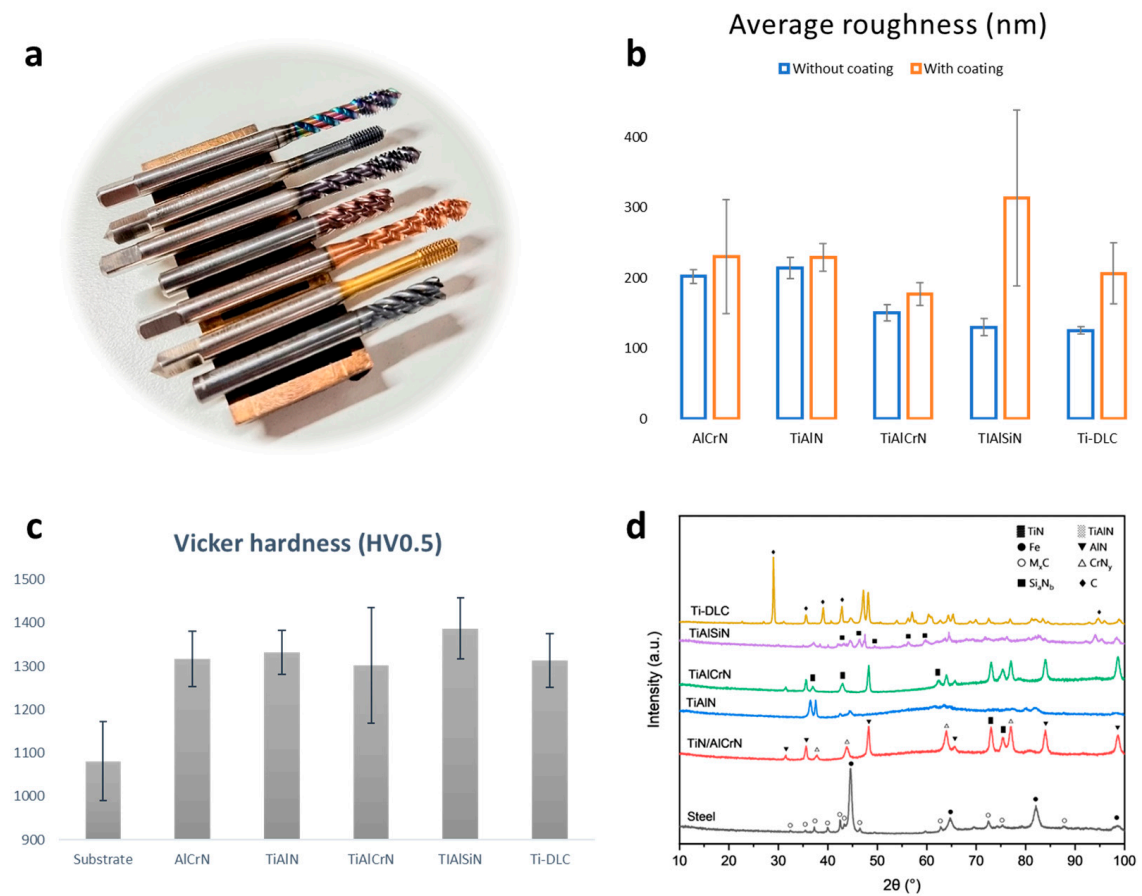


Figure 8. (a) Photograph of samples coated with various coatings. (b) Surface roughness, (c) microhardness measurements, and (d) XRD patterns of HSS substrate, TiN/AlCrN, TiAlN, TiAlCrN, TiAlSiN, and Ti-DLC coating on complex tool samples.

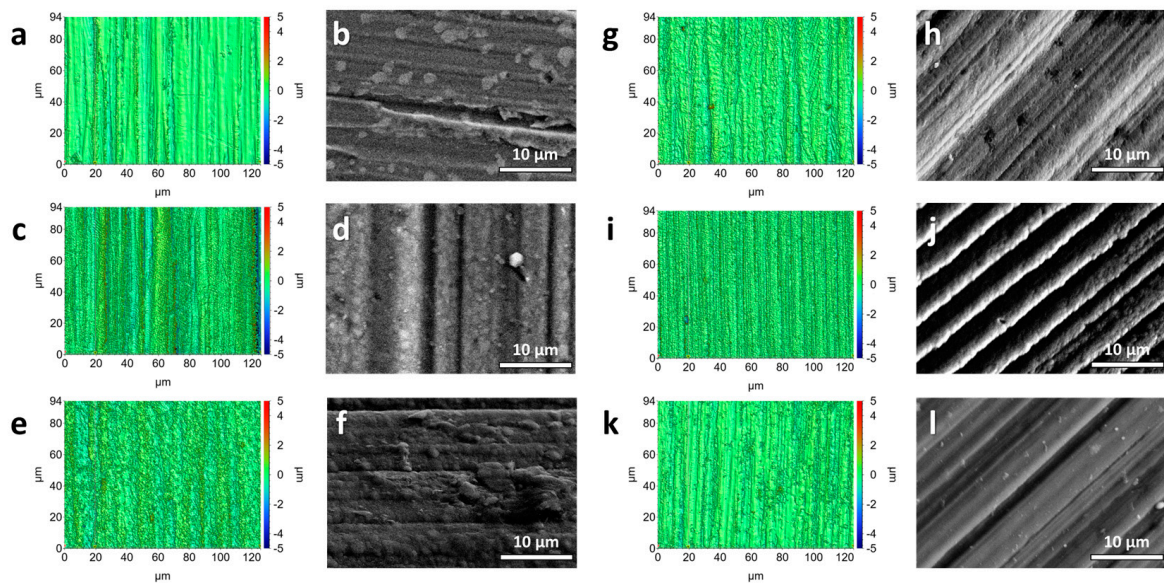


Figure 9. Three-dimensional profilometer and SEM images of (a,b) HSS substrate, (c,d) TiN/AlCrN, (e,f) TiAlN, (g,h) TiAlCrN, (i,j) TiAlSiN, and (k,l) Ti-DLC coatings on complex tool samples.

4. Conclusions

This study provided an in-depth examination of the advantages and drawbacks associated with the implementation of TiN and TiAlN coatings on both flat and complex tool surfaces. In addition, alternate nitride-based options for enhancing wear resistance were investigated. Our findings indicate that the presence of pre-existing surface roughness plays a crucial role in the occurrence of post-coating problems, such as the creation of gas bubbles and uneven distribution of elements. This was observed despite the industrial PVD process adequately promoting consistent coating thickness. Significantly, our research substantiates that properly prepared and polished surfaces prior to the deposition process lead to coatings that exhibit consistent elemental and mechanical characteristics. While industrial coatings may not attain the same level of quality as those produced in laboratory settings, they nonetheless provide satisfactory performance when implemented on a larger scale. These coatings effectively increase hardness, hence improving the resistance of tools to wear under harsh working conditions. In order to enhance the durability and effectiveness of tools, it is imperative to focus on the careful preparation of the initial surface by employing sophisticated polishing and edge preparation methods. Following the optimisation of the substrate, subsequent coating operations could take advantage of these advancements, potentially resulting in substantial reductions in surface roughness and enhancements in overall performance.

Author Contributions: Conceptualisation, M.N.D. and J.W.; methodology, M.N.D.; software, M.N.D.; validation, M.N.D.; formal analysis, M.N.D.; investigation, M.N.D.; resources, M.N.D., A.P., A.M. and J.W.; data curation, M.N.D., S.S., H.J.K., J.H.N.-D. and H.L.; writing—original draft preparation, M.N.D.; writing—review and editing, M.N.D., S.S., J.H.N.-D., H.J.K., H.L., T.G.P., R.K.H., S.A.W. and J.W.; visualisation, M.N.D.; supervision, S.S., R.K.H., S.A.W. and J.W.; project administration, M.N.D., G.S. and J.W.; funding acquisition, G.S. and J.W. All authors have read and agreed to the published version of the manuscript.

Funding: This research was fully funded by the Australian Government through the Australian Research Council Industrial Transformation Training Centre funding scheme, in Surface Engineering for Advanced Materials (SEAM), with project ID IC180100005.

Data Availability Statement: The original contributions presented in the study are included in the article, further in-quiries can be directed to the corresponding author.

Acknowledgments: Minh Nhat Dang wishes to express genuine appreciation to Elena Grebenkina (Elena Dang) for her unwavering emotional support throughout this study endeavour. We acknowledge the unlimited support of Sutton Tools for this project. At last, we acknowledge the assistance of Minh Tien Tran for his hardworking effort during the final peer-review round of this work.

Conflicts of Interest: Author John H. Navarro-Devia, Guy Stephens, Angelo Papageorgiou were employed by the company Sutton Tools. The remaining authors declare that the research was conducted in the absence of any commercial or financial relationships that could be construed as a potential conflict of interest.

References

1. Fox-Rabinovich, G.S.; Kovalev, A.I.; Afanasyev, S.N. Characteristic features of wear in tools made of high-speed steels with surface engineered coatings II: Study of surface engineered high-speed steel cutting tools by AES, SIMS and EELFAS methods. *Wear* **1996**, *198*, 280–286. [[CrossRef](#)]
2. Navarro-Devia, J.H.; Amaya, C.; Caicedo, J.C.; Aperador, W. Performance evaluation of HSS cutting tool coated with hafnium and vanadium nitride multilayers, by temperature measurement and surface inspection, on machining AISI 1020 steel. *Surf. Coat. Technol.* **2017**, *332*, 484–493. [[CrossRef](#)]
3. Bobzin, K. High-performance coatings for cutting tools. *CIRP J. Manuf. Sci. Technol.* **2017**, *18*, 1–9. [[CrossRef](#)]
4. Navarro-Devia, J.H.; Amaya, C.; Caicedo, J.C.; Martínez, J.H.; Aperador, W. Hafnium and vanadium nitride multilayer coatings [HfN/VN]_n deposited onto HSS cutting tools for dry turning of a low carbon steel: A tribological compatibility case study. *Int. J. Adv. Manuf. Technol.* **2019**, *101*, 2065–2081. [[CrossRef](#)]

5. Uddin, G.M.; Joyia, F.M.; Ghufran, M.; Khan, S.A.; Raza, M.A.; Faisal, M.; Arafat, S.M.; Zubair, S.W.H.; Jawad, M.; Zafar, M.Q.; et al. Comparative performance analysis of cemented carbide, TiN, TiAlN, and PCD coated inserts in dry machining of Al 2024 alloy. *Int. J. Adv. Manuf. Technol.* **2021**, *112*, 1461–1481. [[CrossRef](#)]
6. Ortíz, J.; Caicedo, J.; Navarro-Devia, J.; Martínez, J.; Aperador, W. HfN Coating of ASSAB 17 Steel by PVD Method and its Effects on 6063-T5 Aluminum Alloy Turning. *Tribol. Ind.* **2020**, *42*, 679–691. [[CrossRef](#)]
7. Ghantasala, S.B.; Sharma, S. Magnetron Sputtered Thin Films Based on Transition Metal Nitride: Structure and Properties. *Phys. Status Solidi (a)* **2023**, *220*, 2200229. [[CrossRef](#)]
8. Santecchia, E.; Hamouda, A.M.S.; Musharavati, F.; Zalnezhad, E.; Cabibbo, M.; Spigarelli, S. Wear resistance investigation of titanium nitride-based coatings. *Ceram. Int.* **2015**, *41*, 10349–10379. [[CrossRef](#)]
9. Deng, Y.; Chen, W.; Li, B.; Wang, C.; Kuang, T.; Li, Y. Physical vapor deposition technology for coated cutting tools: A review. *Ceram. Int.* **2020**, *46*, 18373–18390. [[CrossRef](#)]
10. Lungu, M.V. An Insight into TiN, TiAlN and AlTiN Hard Coatings for Cutting Tools. *Mat. Sci. Res. India* **2020**, *17*, 87–89. [[CrossRef](#)]
11. Dabees, S.; Mirzaei, S.; Kaspar, P.; Holcman, V.; Sobola, D. Characterization and Evaluation of Engineered Coating Techniques for Different Cutting Tools—Review. *Materials* **2022**, *15*, 5633. [[CrossRef](#)] [[PubMed](#)]
12. Lengauer, W. Transition Metal Carbides, Nitrides, and Carbonitrides. In *Handbook of Ceramic Hard Materials*; Wiley-VCH Verlag GmbH: Weinheim, Germany, 2008; pp. 202–252, ISBN 9780323157223. [[CrossRef](#)]
13. Kuo, C.-C.; Lin, Y.-T.; Chan, A.; Chang, J.-T. High Temperature Wear Behavior of Titanium Nitride Coating Deposited Using High Power Impulse Magnetron Sputtering. *Coatings* **2019**, *9*, 555. [[CrossRef](#)]
14. Chang, Y.-Y.; Weng, S.-Y.; Chen, C.-H.; Fu, F.-X. High temperature oxidation and cutting performance of AlCrN, TiVN and multilayered AlCrN/TiVN hard coatings. *Surf. Coat. Technol.* **2017**, *332*, 494–503. [[CrossRef](#)]
15. Faley, M.I.; Liu, Y.; Dunin-Borkowski, R.E. Titanium Nitride as a New Prospective Material for NanoSQUIDs and Superconducting Nanobridge Electronics. *Nanomaterials* **2021**, *11*, 466. [[CrossRef](#)] [[PubMed](#)]
16. Stone, D.S.; Yoder, K.B.; Sproul, W.D. Hardness and elastic modulus of TiN based on continuous indentation technique and new correlation. *J. Vac. Sci. Technol. A Vac. Surf. Films* **1991**, *9*, 2543–2547. [[CrossRef](#)]
17. Zhang, S.; Zhu, W. TiN coating of tool steels: A review. *J. Mater. Process. Technol.* **1993**, *39*, 165–177. [[CrossRef](#)]
18. Posti, E.; Nieminen, I. Influence of coating thickness on the life of TiN-coated high speed steel cutting tools. *Wear* **1989**, *129*, 273–283. [[CrossRef](#)]
19. Harris, S.G.; Doyle, E.D.; Vlasveld, A.C.; Audy, J.; Quick, D. A study of the wear mechanisms of Ti1-xAlxN and Ti1-x-yAlxCrN coated high-speed steel twist drills under dry machining conditions. *Wear* **2003**, *254*, 723–734. [[CrossRef](#)]
20. Shtansky, D.V.; Levashov, E.A.; Sheveiko, A.N.; Moore, J.J. The Structure and Properties of Ti-B-N, Ti-Si-B-N, Ti-Si-C-N, and Ti-Al-C-N Coatings Deposited by Magnetron Sputtering Using Composite Targets Produced by Self-Propagating High-Temperature Synthesis (SHS). *J. Mater. Synth. Process.* **1998**, *6*, 61–72. [[CrossRef](#)]
21. Steinmann, P.A.; Hintermann, H.E. Adhesion of TiC and Ti(C,N) coatings on steel. *J. Vac. Sci. Technol. A Vac. Surf. Films* **1985**, *3*, 2394–2400. [[CrossRef](#)]
22. Ronkainen, H.; Nieminen, I.; Holmberg, K.; Leyland, A.; Matthews, A.; Matthes, B.; Broszeit, E. Evaluation of some titanium-based ceramic coatings on high speed steel cutting tools. *Surf. Coat. Technol.* **1991**, *49*, 468–473. [[CrossRef](#)]
23. Ezugwu, E.O.; Wang, Z.M. Titanium alloys and their machinability—A review. *J. Mater. Process. Technol.* **1997**, *68*, 262–274. [[CrossRef](#)]
24. Jehn, H.A.; Hofmann, S.; Münz, W.D. Surface and interface characterization of heat-treated (Ti, Al)N coatings on high speed steel substrates. *Thin Solid Films* **1987**, *153*, 45–53. [[CrossRef](#)]
25. Zhao, J.; Liu, Z.; Wang, B.; Hu, J.; Wan, Y. Tool coating effects on cutting temperature during metal cutting processes: Comprehensive review and future research directions. *Mech. Syst. Signal Process.* **2021**, *150*, 107302. [[CrossRef](#)]
26. Chenrayan, V.; Manivannan, C.; Shahapurkar, K.; Krishna, A.; Tirth, V.; Algahtani, A.; Alarifi, I.M. Machinability Performance Investigation of TiAlN-, DLC-, and CNT-Coated Tools during Turning of Difficult-to-Cut Materials. *J. Nanomater.* **2022**, *2022*, 9664365. [[CrossRef](#)]
27. Geometrical Product Specifications (GPS). *Surface Texture: Profile Method—Rules and Procedures for the Assessment of Surface Texture*; International Organization for Standardization: Geneva, Switzerland, 1998.
28. Panjan, P.; Drnovšek, A.; Gselman, P.; Čekada, M.; Panjan, M. Review of Growth Defects in Thin Films Prepared by PVD Techniques. *Coatings* **2020**, *10*, 447. [[CrossRef](#)]
29. Hultman, L. Thermal stability of nitride thin films. *Vacuum* **2000**, *57*, 1–30. [[CrossRef](#)]
30. Ramya, S.; Mudali, U.K. In-situ Raman and X-ray photoelectron spectroscopic studies on the pitting corrosion of modified 9Cr-1Mo steel in neutral chloride solution. *Appl. Surf. Sci.* **2018**, *428*, 1106–1118. [[CrossRef](#)]
31. Dang, M.N.; Nhat Minh, D.; Ngoc Trung, L.; Thanh Hai, N.; Trong Lu, L.; Thi Thanh Tam, L.; Tuan Hong, N.; Van Thao, N.; Ngoc Minh, P.; Ngoc Hong, P. One-Step Synthesis of Molybdenum Oxide/graphene Composites. *VNU J. Sci. Math.-Phys.* **2021**, *37*, 47–53. [[CrossRef](#)]
32. Boucherit, N.; Hugot-Le Goff, A.; Joiret, S. Influence of Ni, Mo, and Cr on Pitting Corrosion of Steels Studied by Raman Spectroscopy. *CORROSION* **1992**, *48*, 569–579. [[CrossRef](#)]

33. Ipaz, L.; Aperador, W.; Caicedo, J.; Esteve, J.; Zambrano, G. A Practical Application of X-Ray Spectroscopy in Ti-Al-N and Cr-Al-N Thin Films. In *X-Ray Spectroscopy*; Sharma, S.K., Ed.; InTech: London, UK, 2012; ISBN 978-953-307-967-7. [[CrossRef](#)]
34. Zhu, S.; Xiao, L.; Cortie, M.B. Surface enhanced Raman spectroscopy on metal nitride thin films. *Vib. Spectrosc.* **2016**, *85*, 146–148. [[CrossRef](#)]
35. Kosari Mehr, A.; Babaei, R.; Mehr, A.K.; Zamani Meymian, M.R. Raman and ultraviolet–visible spectroscopy of titanium chromium nitride thin films. *Surf. Eng.* **2021**, *37*, 148–153. [[CrossRef](#)]
36. Das, S.; Guha, S.; Ghadai, R.; Kumar, D.; Swain, B.P. Structural and mechanical properties of CVD deposited titanium aluminium nitride (TiAlN) thin films. *Appl. Phys. A* **2017**, *123*, 412. [[CrossRef](#)]
37. Ponon, N.K.; Appleby, D.J.R.; Arac, E.; King, P.J.; Ganti, S.; Kwa, K.S.K.; O’Neill, A. Effect of deposition conditions and post deposition anneal on reactively sputtered titanium nitride thin films. *Thin Solid Films* **2015**, *578*, 31–37. [[CrossRef](#)]
38. Shum, P.W.; Li, K.Y.; Zhou, Z.F.; Shen, Y.G. Structural and mechanical properties of titanium–aluminium–nitride films deposited by reactive close-field unbalanced magnetron sputtering. *Coat. Technol.* **2004**, *185*, 245–253. [[CrossRef](#)]
39. Barshilia, H.C.; Rajam, K.S. Raman spectroscopy studies on the thermal stability of TiN, CrN, TiAlN coatings and nanolayered TiN/CrN, TiAlN/CrN multilayer coatings. *J. Mater. Res.* **2004**, *19*, 3196–3205. [[CrossRef](#)]
40. Constable, C.P.; Yarwood, J.; Münz, W.-D. Raman microscopic studies of PVD hard coatings. *Surf. Coat. Technol.* **1999**, *116–119*, 155–159. [[CrossRef](#)]
41. Spengler, W.; Kaiser, R.; Christensen, A.N.; Müller-Vogt, G. Raman scattering, superconductivity, and phonon density of states of stoichiometric and nonstoichiometric TiN. *Phys. Rev. B* **1978**, *17*, 1095–1101. [[CrossRef](#)]
42. Yazdani, A.; Soltanieh, M.; Aghajani, H.; Rastegari, S. A new method for deposition of nano sized titanium nitride on steels. *Vacuum* **2011**, *86*, 131–139. [[CrossRef](#)]
43. Zhang, P.; Chen, Y.; Xiao, W.; Ping, D.; Zhao, X. Twin structure of the lath martensite in low carbon steel. *Prog. Nat. Sci. Mater. Int.* **2016**, *26*, 169–172. [[CrossRef](#)]
44. Carbonari, M.J.; Martinelli, J.R. Effects of hot isostatic pressure on titanium nitride films deposited by physical vapor deposition. *Mat. Res.* **2001**, *4*, 163–168. [[CrossRef](#)]
45. Danışman, Ş.; Odabaş, D.; Teber, M. The Effect of TiN, TiAlN, TiCN Thin Films Obtained by Reactive Magnetron Sputtering Method on the Wear Behavior of Ti6Al4V Alloy: A Comparative Study. *Coatings* **2022**, *12*, 1238. [[CrossRef](#)]
46. Bonu, V.; Jeevitha, M.; Praveen Kumar, V.; Srinivas, G.; Siju; Barshilia, H.C. Solid particle erosion and corrosion resistance performance of nanolayered multilayered Ti/TiN and TiAl/TiAlN coatings deposited on Ti6Al4V substrates. *Surf. Coat. Technol.* **2020**, *387*, 125531. [[CrossRef](#)]
47. Ghorbani, M.M.; Taherian, R.; Mohammadi, M.; Bozorg, M. Investigation of physical and electrical properties of TiN-coated SS316L as bipolar plate of proton exchange membrane fuel cells. *Surf. Eng.* **2021**, *37*, 822–830. [[CrossRef](#)]
48. Vaca, L.S.; Quintana, J.P.; Guitar, M.A.; Vega, D.; Brühl, S.P.; Márquez, A. Influence of the Pre-Treatments and Process Temperature on the Adhesion of TiN Films Deposited by PBII&D Over Nitrided Austenitic Stainless Steel. *Mat. Res.* **2019**, *22*, e20190282. [[CrossRef](#)]
49. Zhang, H.; Li, F.; Jia, Q. Preparation of titanium nitride ultrafine powders by sol–gel and microwave carbothermal reduction nitridation methods. *Ceram. Int.* **2009**, *35*, 1071–1075. [[CrossRef](#)]
50. Marlo, M.; Milman, V. Density-functional study of bulk and surface properties of titanium nitride using different exchange-correlation functionals. *Phys. Rev. B* **2000**, *62*, 2899–2907. [[CrossRef](#)]
51. Sharifi Malvajerdi, S.; Sharifi Malvajerdi, A.; Ghanaatshoar, M.; Habibi, M.; Jahdi, H. TiCrN-TiAlN-TiAlSiN-TiAlSiCN multi-layers utilized to increase tillage tools useful lifetime. *Sci. Rep.* **2019**, *9*, 19101. [[CrossRef](#)]
52. Cheong, J.Y.; Ding, X.Z.; Tay, B.K.; Zeng, X.T. Thermal Stability and Oxidation Resistance of CrAlSiN Nano-Structured Coatings Deposited by Lateral Rotating Cathode Arc. *Key Eng. Mater.* **2010**, *447–448*, 725–729. [[CrossRef](#)]
53. Sampath Kumar, T.; Balasivanandha Prabu, S.; Manivasagam, G. Metallurgical Characteristics of TiAlN/AlCrN Coating Synthesized by the PVD Process on a Cutting Insert. *J. Mater. Eng. Perform.* **2014**, *23*, 2877–2884. [[CrossRef](#)]
54. Bartosik, M.; Rumeau, C.; Hahn, R.; Zhang, Z.L.; Mayrhofer, P.H. Fracture toughness and structural evolution in the TiAlN system upon annealing. *Sci. Rep.* **2017**, *7*, 16476. [[CrossRef](#)]
55. Grzesik, W.; Małacka, J. The Oxidation Behaviour and Notch Wear Formation of TiAlN Coated Tools Using Different Oxidation Techniques. *Materials* **2021**, *14*, 1330. [[CrossRef](#)] [[PubMed](#)]
56. Thi Le, T.-L.; Nguyen, L.T.; Nguyen, H.-H.; Nghia, N.V.; Vuong, N.M.; Hieu, H.N.; Thang, N.V.; Le, V.T.; Nguyen, V.H.; Lin, P.-C.; et al. Titanium Nitride Nanodonuts Synthesized from Natural Ilmenite Ore as a Novel and Efficient Thermoplasmonic Material. *Nanomaterials* **2020**, *11*, 76. [[CrossRef](#)] [[PubMed](#)]
57. Madan, A.; Kim, I.W.; Cheng, S.C.; Yashar, P.; Dravid, V.P.; Barnett, S.A. Stabilization of Cubic AlN in Epitaxial AlN/TiN Superlattices. *Phys. Rev. Lett.* **1997**, *78*, 1743–1746. [[CrossRef](#)]
58. Bouabibsa, I.; Lamri, S.; Sanchette, F. Structure, Mechanical and Tribological Properties of Me-Doped Diamond-Like Carbon (DLC) (Me = Al, Ti, or Nb) Hydrogenated Amorphous Carbon Coatings. *Coatings* **2018**, *8*, 370. [[CrossRef](#)]
59. Pang, H.; Wang, X.; Zhang, G.; Chen, H.; Lv, G.; Yang, S. Characterization of diamond-like carbon films by SEM, XRD and Raman spectroscopy. *Appl. Surf. Sci.* **2010**, *256*, 6403–6407. [[CrossRef](#)]

60. Li, G.; Li, L.; Han, M.; Luo, S.; Jin, J.; Wang, L.; Gu, J.; Miao, H. The Performance of TiAlSiN Coated Cemented Carbide Tools Enhanced by Inserting Ti Interlayers. *Metals* **2019**, *9*, 918. [[CrossRef](#)]
61. Demir, H.; Gullu, A.; Ciftci, I.; Seker, U. An Investigation into the Influences of Grain Size and Grinding Parameters on Surface Roughness and Grinding Forces when Grinding. *J. Mech. Eng.* **2010**, *56*, 447–454.

Disclaimer/Publisher’s Note: The statements, opinions and data contained in all publications are solely those of the individual author(s) and contributor(s) and not of MDPI and/or the editor(s). MDPI and/or the editor(s) disclaim responsibility for any injury to people or property resulting from any ideas, methods, instructions or products referred to in the content.